Bioelectrochemistry 127 (2019) 125–135

Contents lists available at ScienceDirect

Bioelectrochemistry

journal homepage: www.elsevier.com/locate/bioelechem

Sensitive amperometric biosensors for detection of glucose and cholesterol using a platinum/reduced graphene oxide/poly(3-aminobenzoic acid) film-modified screen-printed carbon electrode

Sopit Phetsang [a,b], Jaroon Jakmunee [a,d,e], Pitchaya Mungkornasawakul [a,d,f,*], Rawiwan Laocharoensuk [c,**], Kontad Ounnunkad [a,d,e,*]

[a] Department of Chemistry, Faculty of Science, Chiang Mai University, Chiang Mai 50200, Thailand
[b] The Graduate School, Chiang Mai University, Chiang Mai 50200, Thailand
[c] Nanostructures and Functional Assembly Laboratory (NFA), National Nanotechnology Center (NANOTEC), National Science and Technology Development Agency (NSTDA), Pathum Thani 12120, Thailand
[d] Center of Excellence for Innovation in Chemistry (PERCH-CIC), Faculty of Science, Chiang Mai University, Chang Mai 50200, Thailand
[e] Research Center on Chemistry for Development of Health Promoting Products from Northern Resources, Chiang Mai University, Chiang Mai 50200, Thailand
[f] Environmental Science Research Center (ESRC), Faculty of Science, Chiang Mai University, Chiang Mai 50200, Thailand

ARTICLE INFO

Article history:
Received 8 November 2018
Received in revised form 30 January 2019
Accepted 31 January 2019
Available online 13 February 2019

Keywords:
Glucose biosensor
Cholesterol biosensor
Platinum
Reduced graphene oxide
Screen printed carbon electrode
Electrodeposition

ABSTRACT

A facile one-step electrochemical synthesis of a platinum/reduced graphene oxide/poly(3-aminobenzoic acid) (Pt/rGO/P3ABA) nanocomposite film on a screen-printed carbon electrode (SPCE) and its application in the development of sensitive amperometric biosensors was successfully demonstrated herein. The electropolymerization of P3ABA together with co-electrodeposition of rGO and Pt was conducted by cyclic voltammetry, as was the GO reduction to rGO. A Pt/rGO/P3ABA-modified SPCE exhibited excellent electrocatalytic oxidation towards hydrogen peroxide (H_2O_2) and can be employed as an electrochemical platform for the immobilization of glucose oxidase (GOx) and cholesterol oxidase (ChOx) to fabricate glucose and cholesterol biosensors, respectively. Under the optimized conditions at a working potential of +0.50 V, the proposed biosensors revealed excellent linear responses to glucose and cholesterol in the concentration ranges of 0.25–6.00 mM and 0.25–4.00 mM, respectively, with high sensitivities of 22.01 and 15.94 μA mM^{-1} cm^{-2} and low detection limits (LODs) of 44.3 and 40.5 μM. Additionally, the Michaelis-Menten constant (K_m) of GOx was 3.54 mM, while the K_m of ChOx was 3.82 mM. Both biosensors displayed a good anti-interference ability and clearly exhibited acceptable recoveries for the detection of glucose and cholesterol in a human serum sample (98.2–104.1%).
© 2019 Published by Elsevier B.V.

1. Introduction

The estimation and management of glucose and cholesterol metabolite levels in human blood are very important to clinical diagnostics because an abnormality of either metabolite level can lead to high risks of several serious diseases [1,2]. It is well known that diabetes mellitus is a chronic disease associated with abnormally high levels of glucose. This disease is a global public health problem and is one of the main factors for mortality and disability due to its long-term complications including blindness, kidney failure, heart disease, and cardiovascular disease [2–5]; at the same time, a high level of cholesterol in the blood also causes heart disease and other diseases such as arteriosclerosis, hypertension, coronary artery disease, and cerebral thrombosis [1,6]. Furthermore, the determination of both glucose and cholesterol has been essentially required for nutritional quality controls in the food and beverage industries [7,8].

Various conventional approaches including chromatographic [8–10], spectrophotometric [11,12], chemiluminescence [13,14], and electrochemical methods [15–17] have been developed to determine glucose and cholesterol in actual samples. Among these techniques, an electrochemical biosensor represents an excellent potential tool and has attracted much attention as a point-of-care (POC) device because of its accurate and rapid analysis, high sensitivity and specificity, ease of use, portable equipment and low cost [15]. Typically, electrochemical biosensors of glucose and cholesterol can be achieved by the enzymatic reaction between an analyte and oxidase enzyme, i.e., glucose oxidase (GOx) and cholesterol oxidase (ChOx), due to high specificity. In this

* Corresponding authors at: Department of Chemistry, Faculty of Science, Chiang Mai University, Chiang Mai 50200, Thailand.
** Corresponding author at: Nanostructures and Functional Assembly Laboratory (NFA), National Nanotechnology Center (NANOTEC), National Science and Technology Development Agency (NSTDA), Pathum Thani 12120, Thailand.
E-mail addresses: pitchaya16@gmail.com (P. Mungkornasawakul), rawiwan.lao@nanotec.or.th (R. Laocharoensuk), suriyacmu@yahoo.com (K. Ounnunkad).

https://doi.org/10.1016/j.bioelechem.2019.01.008
1567-5394/© 2019 Published by Elsevier B.V.

case, the quantification of glucose and cholesterol can be electrochemically investigated by monitoring the concentration of hydrogen peroxide (H_2O_2) generated during the enzymatic reaction [18,19].

Nanomaterials are the most promising candidates that have been applied as support materials in various kinds of biosensors due to their outstanding physical and chemical properties including high surface area to volume ratio, good thermal and electrical properties, and high conductivity [20,21]. Therefore, the modification of nanostructured materials on the electrode surface has been widely performed in order to improve the electrochemical performances of the devices. Graphene (GP), an aromatic carbon monolayer nanomaterial, is considerably attractive among the various types of carbon nanostructures because it possesses many advantageous features such as excellent mobility of electron transfer, good electrical conductivity, ultralight weight, large surface area and high mechanical strength [20,22]. GP is primarily obtained from the chemical reduction of graphene oxide (GO) by many reducing agents including sodium borohydride [23], hydrazine [24], and ammonia [25]; however, these reagents are toxic. Moreover, nontoxic reducing agents including ascorbic acid [26], hydroquinone [27], and glucose [28] have also been employed. Nevertheless, GP can easily aggregate and restack to form graphitic particles via van der Waals interactions and π-π stacking from the reduction process [29]. Consequently, electrochemical reduction is a candidate procedure for GP preparation [30–33]. This method is usually performed under mild conditions, which would prevent an agglomeration of GP during the reduction process and reduce the use of toxic reagents.

Functionalization of nanomaterials plays a significant role in the improvement of biosensor performance by providing greater electrochemical properties including high electron transfer, good conductivity and better biocompatibility compared with those of a single component. Recently, the combination of GP with other nanostructures such as metal oxides, metal nanoparticles and/or conducting polymers has been performed to obtain nanocomposites possessing attractive, enhanced properties. A variety of nanocomposites based on GP sheets, such as Pt/GP [18,34–36], GP/polyaniline [20], and Pt/GP–CNT [37], have been extensively employed in electrochemical sensors and exhibit an excellent electrocatalytic effect towards H_2O_2. The insertion of metallic nanoparticles into GP nanostructures leads to enhanced conductivity and electrocatalytic properties; additionally, the introduction of polymers or conducting polymers (CPs), such as polyaniline, chitosan, and poly(aminobenzoic acid), into the composites has contributed to the production of abundant functional groups such as amines and carboxylic groups, which can be used as support materials for the immobilization of biomolecules via covalent binding [15,38–42]. The immobilization of GOx or ChOx on electrodes modified with Pt/GP [18,43], GP/chitosan [44], PtPd/GP/chitosan [16], Pt/GP/chitosan [45], AuNPs/GP/polyaniline [39], and GP/polyvinyl pyrrolidone/polyaniline [46] has been successfully performed for applications as glucose and cholesterol biosensors, respectively. These nanocomposites demonstrated an improved chemical stability, greater electrical conductivity and larger surface area, which can promote more rapid electron transfer into the system through an advanced synergistic effect; such materials are importantly useful in many fields of electroanalytical sciences [15]. On the other hand, the preparation of these nanocomposites is much more complicated than conventional methods, requiring more numerous chemicals and greater time consumption.

In this work, a facile preparation of a sensing platform based on a platinum/reduced graphene oxide/poly(3-aminobenzoic acid) (Pt/rGO/P3ABA) nanocomposite has been successfully developed for using the modified electrode as a glucose and cholesterol biosensor. A new one-step electrochemical synthesis of a Pt/rGO/P3ABA nanocomposite film was performed by cyclic voltammetry (CV). Under the electrochemical processing, GO was reduced to rGO at the cathodic potential, while the polymerization of P3ABA was achieved at the anodic potential, and Pt nanoparticles (PtNPs) were electrodeposited during the scanning process. The proposed Pt/rGO/P3ABA sensing platform obtained multifunctional properties, and Pt distributed on the rGO sheet provided a higher surface area and displayed an excellent electrocatalytic effect towards H_2O_2. Additionally, the biocompatible P3ABA contains an abundance of carboxylic groups, which are used as the matrix for immobilization of enzymes (GOx or ChOx) via amide linkages to increase enzyme loading, to enhance the sensitivity and specificity and to improve the stability of the modified electrode. Furthermore, the biosensing platform retains the bioactivity of the enzymes and exhibits a great potential for measurement of glucose and cholesterol in biological fluids with high sensitivity.

2. Experimental details

2.1. Materials and reagents

All chemicals used were of analytical grade. Glucose oxidase (GOx) 10 KU from *Aspergillus niger* Type VII, cholesterol oxidase (ChOx) 250 UN from *Streptomyces* sp. EC 1.1.3.6, D(+)-glucose (Glu, ≥ 99.5%), cholesterol (Cho, ≥ 99%), uric acid (UA, ≥ 99%), L-ascorbic acid (AA, 99%), 3-aminobenzoic acid (3ABA, 98%), chloroplatinic acid solution (H_2PtCl_6, 8 wt%), potassium chloride (KCl, 99.5%), sodium chloride (NaCl, 99.5%), disodium hydrogen phosphate (Na_2HPO_4, 99.5%), potassium dihydrogen phosphate (KH_2PO_4, 99.5%), and human serum from human male (AB plasma, USA origin) were purchased from Sigma-Aldrich (Singapore). Potassium ferricyanide ($K_3[Fe(CN)_6]$, ≥ 99%), N-(3-dimethylaminopropyl)-N′-ethylcarbodiimide hydrochloride (EDC, ≤ 100%), and N-hydroxysuccinimide (NHS, ≥ 99%) were obtained from Merck (Germany). Sucrose (extra pure), sodium dodecyl sulfate (SDS, 96%), and polyoxyethylene octyl phenyl ether (Triton X-100, extra pure) were purchased from Loba Chemie (India). Hydrochloric acid (HCl, 37%) and isopropanol (>99%) were obtained from RCI Labscan (Thailand). Hydrogen peroxide (H_2O_2, 30%) was purchased from QRëC (Thailand). Natural graphite (≥ 98%) was purchased from Bay Carbon Inc., USA. All other chemicals were of analytical reagent (AR) grade. Deionized water (DI) was collected from a purification system (Millipore systems, USA). Stock solutions of GOx and ChOx were freshly prepared in phosphate buffered saline (PBS) solution. A stock solution of glucose was prepared daily with DI water and stored overnight before use for the mutarotation determination [5]. The GO was synthesized from natural graphite using a modified Hummers method [47]. The stock solution of cholesterol was prepared by dissolving cholesterol in a mixture solution of Triton X-100 (1.0 mL), isopropanol (1.0 mL), and DI water (18 mL) at a temperature of 60 °C under stirring to obtain a standard solution [48]. The stock solutions were diluted to create different concentrations of analytes with PBS (pH 7.4) for further experimentation. The human serum solution was employed with a 50-fold dilution.

2.2. Apparatus and electrodes

Electrochemical measurements, i.e., cyclic voltammetry (CV) and chronoamperometry, were carried out with an EmStat3 potentiostat (PalmSens, Netherlands). Electrochemical impedance spectroscopy (EIS) was performed on an electrochemical impedance analyzer, a Z100 EDAQ potentiostat (Australia). Screen-printed carbon electrodes (SPCEs) were purchased from Zensor, USA. The SPCE is composed of a carbon working electrode (WE) with a diameter of 3.0 mm, carbon counter electrode (CE), and silver/silver chloride (Ag/AgCl) pseudo-reference electrode (RE). All experiments were measured at room temperature. The SPCEs were treated by employing a plasma cleaner (PDC-32G) prior to use. A field-emission scanning electron microscope (FE-SEM, JEOL JSM-6335F) combined with energy dispersive X-ray spectroscopy (EDS) was employed for studying the surface morphology of our synthesized nanostructures and elemental analysis of the sample surfaces.

2.3. Procedures

2.3.1. Preparation of Pt/rGO/P3ABA-modified SPCE

A 0.50 mg mL^{-1} GO suspension was prepared in 0.50 M HCl by ultrasonication for 1 h. Then, H_2PtCl_6 and 3-aminobenzoic acid (3ABA) monomer were added into the GO suspension and sonicated for 1 h to obtain a homogeneous dispersion. The solution contained 0.50 mg mL^{-1} GO, 2.5 mM H_2PtCl_6, and 50 mM 3ABA. In the first step, SPCE was treated in a plasma cleaner for removing impurities and improving the hydrophilic property, followed by immersing the SPCE into a mixture solution. The mixture suspension was electrochemically deposited onto WE using CV by applying the potential between 1.20 and − 0.80 V at a scan rate of 100 mV s^{-1} for 10 cycles. The deposition was conducted under stirring at 700 rpm. The Pt/rGO/P3ABA-modified electrode was rinsed with DI water several times and then dried at room temperature. In the cases of rGO/P3ABA- and Pt/P3ABA-modified SPCEs, the suspension was prepared according to the same procedure with absence of the precursor, H_2PtCl_6 and GO, respectively, and only 3ABA was included in the deposition solution to prepare the P3ABA-modified SPCE. All electrodepositions were performed under similar conditions.

2.3.2. Fabrication of glucose and cholesterol biosensors

The best modified electrode, denoted as Pt/rGO/P3ABA-modified SPCE, was incubated with 10 μL of 0.40 M EDC/0.10 M NHS (1:1 *v*/v) solution for 20 min to activate the carboxylic group of the P3ABA on the surface electrode; then, the electrode was rinsed with DI water several times and dried at room temperature. For the fabrication of the glucose biosensor, 2.5 μL of GOx solution (5 mg mL^{-1}) was dropped onto the modified electrode, while 2.5 μL of ChOx solution (0.2 UμL^{-1}) was drop-casted onto the electrode for construction of the cholesterol biosensor. Then, the GOx/Pt/rGO/P3ABA-modified SPCE and ChOx/Pt/rGO/P3ABA-modified SPCE were stored at a temperature of 4.0 °C overnight for further use. A schematic diagram of the device fabrication, together with the enzymatic reactions, is demonstrated in Fig. 1. For testing the applicability of our optimized electrode, glucose and cholesterol spiked in diluted human serum samples were used.

2.3.3. Electrochemical measurements

The electron transfer processes of the Pt/rGO/P3ABA-, Pt/P3ABA-, rGO/P3ABA-, and P3ABA-modified SPCEs were studied using CV and EIS measurements in 5.0 mM $K_3[Fe(CN)_6]$ solution containing 0.10 M KCl. The CV was undertaken by scanning the potential from 0.80 to −0.40 V at a scan rate of 50 mV s^{-1}. Additionally, the effect of scan rate on the electrochemical response of the Pt/rGO/P3ABA-modified SPCE was investigated. Moreover, the sensitivity of different modified SPCEs for the electrooxidation of H_2O_2 was investigated using CV in a 2.50 mM H_2O_2 solution under a scanning potential from −0.20 to 0.80 V at a scan rate of 50 mV s^{-1}. Under the optimized conditions, amperometry was conducted for the successive addition of H_2O_2 solution into 0.10 M PBS (pH 7.4) under stirring at an applied potential of +0.50 V at the electrodes. In addition, the presence of PtNPs within the nanocomposite film was evaluated in 0.50 M H_2SO_4 using CV with the scan potential from −0.30 to 1.20 V at a scan rate of 50 mV s^{-1}. The quantitative analysis of glucose or cholesterol standard solution was performed via the detection of H_2O_2, which is one of the products from the enzymatic reaction, and the measurement was operated using chronoamperometry at a potential of +0.50 V for 100 s. All electrochemical studies were performed at room temperature. Moreover, the detection of both analytes added into diluted human serum was carried out using the same potential.

3. Results and discussion

3.1. Optimization of electrochemical synthesis

In this work, a nanocomposite film of Pt/rGO/P3ABA-modified SPCE was successfully synthesized by a one-pot electrochemical deposition via CV, and the cyclic voltammograms (CVs) are demonstrated in Fig. S1 (supporting information). The CV was performed over the potential range between −0.80 and 1.20 V, in which 3ABA in an electrolytic

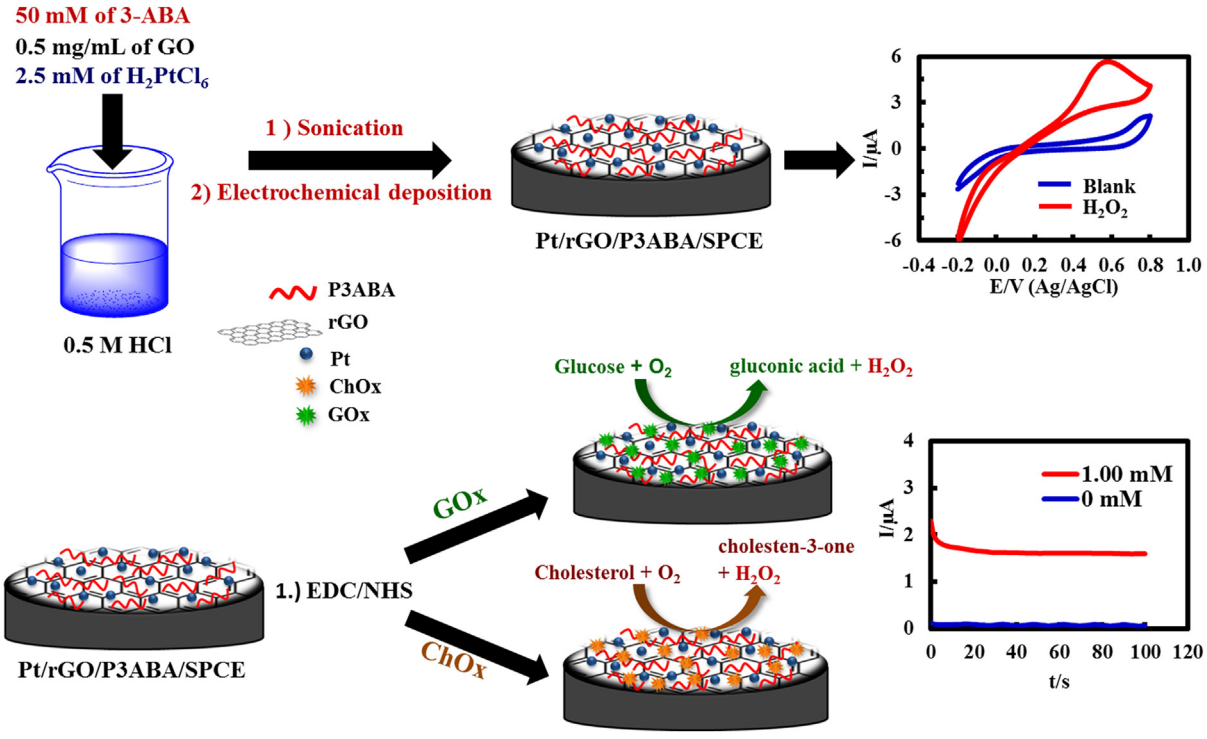

Fig. 1. Schematic representation of the fabrication of glucose and cholesterol biosensors and the enzymatic reaction mechanism of biosensors based on the Pt/rGO/P3ABA nanocomposite film-modified SPCE.

solution was electropolymerized to form poly(3-aminobenzoic acid) (P3ABA) on the SPCE. The electrooxidation of 3ABA initially occurs at the potential of ca. +0.85 V, after which, P3ABA forms on the electrode surface [49,50]. Moreover, during polymerization, GO and PtNPs were also electrochemically deposited onto SPCEs, and GO was reduced to rGO under the negative potential scan [51]. For codeposition of PtNPs, during deposition of the nanocomposite film, the electrochemical profile of Pt was observed. Pt is oxidized to Pt oxides, which are formed at the anodic peak potential of +0.85 V, and for the reduction to Pt, the cathodic peak current could be clearly observed at the potential of +0.40 V. A well-defined hydrogen adsorption/desorption characteristic is also demonstrated in CV scans over the potential ranges from −0.26 to −0.12 V and − 0.16 to −0.25 V, respectively, which is catalyzed by PtNPs sitting upon the modified SPCE. In addition, the reduction of GO could be achieved at −0.62 V and further negative potential scanning. The irreversible cathodic current peak indicates the reduction of the oxygenated groups on the GO surface under this experimental condition. By increasing the number of CV scans, the nanocomposite amount gradually grows on the SPCE, as seen in the increased peak currents. The concentrations of GO and H_2PtCl_6 for the synthesis exhibited an important effect on the sensitivity of H_2O_2 detection. To obtain the highest current response of the electrocatalysis of H_2O_2, the optimizations of GO and H_2PtCl_6 concentrations were investigated under a fixed concentration of 3ABA monomer at 50 mM. The optimized GO concentration in the monomer solution was observed at 0.50 mg mL^{-1}, which gave the highest sensitivity to H_2O_2, as presented in Fig. S2(A) (supporting information). Moreover, the effect of Pt precursor concentration has also been examined, as shown in Fig. S2(B). As a result, it is noticed that 2.5 mM is the optimal H_2PtCl_6 concentration. In the case of lower concentrations (0.5 or 1.0 mM), the film would contain a smaller deposition amount of PtNPs, thus leading to attenuated electrocatalysis. In contrast, an agglomeration of PtNPs could easily occur at concentrations above 2.5 mM, which would result in a decrease in electrocatalytic efficiency. Consequently, a solution containing 0.50 mg mL^{-1} GO, 2.5 mM H_2PtCl_6, and 50 mM 3-ABA was employed to investigate the number of CV scans necessary for the fabrication of the Pt/rGO/P3ABA film-modified SPCE. The thickness of the polymer film could be subsequently controlled by setting the number of cycles and the scan rate during electrochemical operation [52]. Due to the lower electrochemical reactivity of P3ABA, the increased thickness would restrict the electron transfer or electrochemical reaction at the electrode surface, thus lowering the current response. It was found that after 10 polymerization cycles, the film exhibited a maximum current response to H_2O_2 (Fig. S2(C), supporting information). Therefore, this condition was further used for all experiments of our biosensor development.

3.2. Study of surface morphology

The surface morphologies of different modified electrodes, including the bare SPCE and P3ABA-, Pt/P3ABA-, rGO/P3ABA-, and Pt/rGO/P3ABA-modified SPCEs, were elucidated by SEM, as presented in Figs. 2(A-E) and Figs. S3(A-J) (supporting information). In comparison with those of the bare electrode, the SEM images revealed the morphology change after electrochemical deposition was carried out. As seen in Fig. 2(B), larger particles were observed for the P3ABA-modified SPCE due to covering by P3ABA, while no significant change in particle size was observed on the Pt/P3ABA-modified SPCE surface (Fig. 2(C)) due to polymerization of P3ABA together with PtNPs. Furthermore, the rGO/P3ABA-modified SPCE (Fig. 2(D)) manifestly illustrated flat and flake-like particles and wrinkles on the surface, which is the characteristic structure of rGO [20,53] deposited along with P3ABA. Additionally, the PtNPs/P3ABA coating together with some naked rGO particles and coated rGO particles formed the Pt/rGO/P3ABA nanocomposite, as shown in Fig. 2(E). As a result, it is expected that the nanostructures deposited onto the electrode surface would exhibit a high surface-to-volume ratio (or electroactive surface area), thus facilitating the electron transfer. Moreover, the images of energy dispersive X-ray spectrometry (EDS) elemental mapping for the surfaces of the Pt/P3ABA- and Pt/rGO/P3ABA-modified SPCEs have also been analyzed to confirm the presence of PtNPs, as shown in Fig. S4 and Fig. S5 (supporting information), respectively. It was found that the distribution of Pt was observed in both nanocomposite films (Figs. S4(D) and S5(D), supporting information).

3.3. Electrochemical characterization

3.3.1. Electrochemical activity of prepared modified electrodes

CV was carried out to evaluate the electron transfer properties of different modified electrodes, namely, the bare SPCE and P3ABA-, Pt/P3ABA-, rGO/P3ABA-, and Pt/rGO/P3ABA-modified SPCEs, in contact with 0.10 M KCl solution containing 5.0 mM of $K_3[Fe(CN)_6]$. The experiment was recorded over the potential range from 0.80 V to −0.40 V

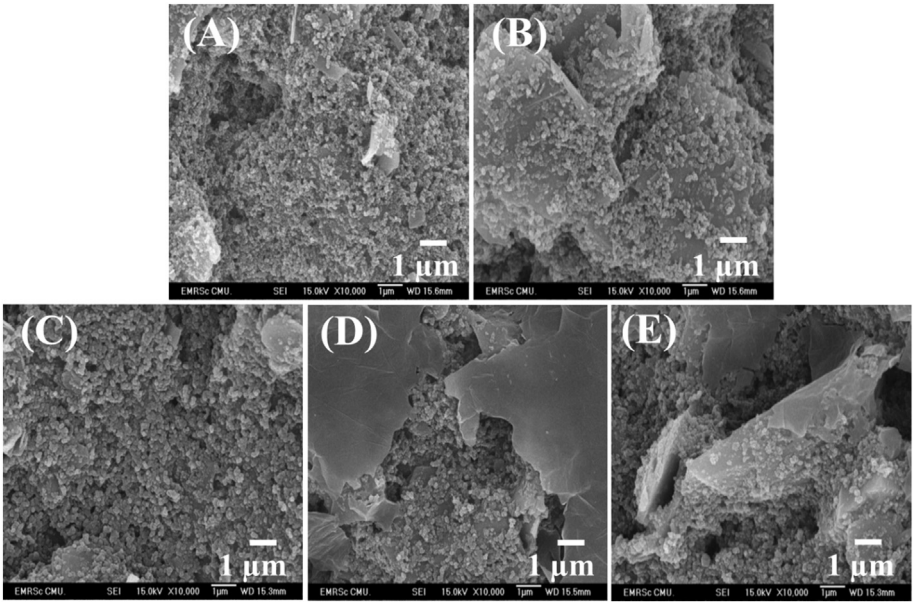

Fig. 2. FE-SEM images of the bare SPCE (A) and P3ABA- (B), Pt/P3ABA- (C), rGO/P3ABA- (D), and Pt/rGO/P3ABA-modified (E) SPCEs.

with the scan rate of 50 mV s^{-1}, and the CVs are presented in Fig. 3(A). As a result, it is clearly seen that all modified electrodes exhibited well-defined redox response peaks and that the different interfacial structures resulted in a significant difference in the electrochemical responses. In the case of bare SPCE, the highest anodic and cathodic peak currents with a peak potential separation (ΔE_p) of 100 mV were observed (curve a, Fig. 3(A)). After P3ABA was electropolymerized on the SPCE, the CV curve was drastically changed, with lower conductivity and a remarkable increase in the ΔE_p value (650 mV) compared to that of the unmodified electrode, indicating the successful formation of polymer film (curve b, Fig. 3(A)). A decrease in redox current responses could have resulted from a higher resistance of electron transfer kinetics at the P3ABA film. Moreover, the Pt/P3ABA-modified SPCE and rGO/P3ABA-modified SPCE exhibited higher redox peaks with declining ΔE_p values of 375 and 450 mV, respectively. It is plausible that the presence of PtNPs or rGO within the deposited P3ABA film caused increased electrocatalytic activities (curves c and d, Fig. 3(A)). Interestingly, a significant improvement of the reversible electrochemical response for the $K_3[Fe(CN)_6]$ redox couple was obviously observed at the Pt/rGO/P3ABA-modified electrode, thus exhibiting a lower ΔE_p value of 200 mV (curve e, Fig. 3(A)). This result suggests that the Pt/rGO/P3ABA nanocomposite can increase the electroactive surface area and improve the electron transfer kinetics due to the distribution of the PtNP catalyst on the rGO and P3ABA surface [23].

EIS was applied to investigate the electron transfer properties of the different surface-modified electrodes, which was measured in the presence of 5.0 mM of $K_3[Fe(CN)_6]$ in 0.10 M KCl solution. EIS was operated under diffusion-kinetic-controlled parameters, and the Nyquist plots are illustrated in Fig. 3(B). Semicircle curves in the plots were clearly observed for all of the devices, corresponding to the resistance of electron transfer within the system [13]. Generally, the charge transfer resistance (R_{ct}) of the electrode surface is equal to the semicircle diameter of the Nyquist diagram [13,51]. As a result, it can be noted that the different modified electrodes exhibited impedance spectra in agreement with their CV characteristics, as mentioned above. The smallest semicircle curve could be observed on the bare SPCE (R_{ct} = 7.75 kΩ, curve a, Fig. 3(B)), implying the lowest resistance of the electron transfer of the redox probe at the electrolyte/electrode interface. On the other hand, the modification of P3ABA onto the SPCE provided the highest charge transport resistance (R_{ct} = 10.0 kΩ, curve b, Fig. 3(B)) compared to those of other electrodes. In this case, the polymer film obviously demonstrated a relatively larger resistance resulting from its low electrical conductivity. To understand the roles of rGO and PtNPs, the Pt/P3ABA- and rGO/P3ABA-modified electrodes were consequently evaluated. As seen in Fig. 3(B) (curves c and d), the R_{ct} value was decreased to the resistances of 8.75 kΩ and 9.0 kΩ for Pt/P3ABA and rGO/P3ABA, respectively, indicating that loading PtNPs and rGO into nanocomposites could improve the conductivity and facilitate the electron transfer. Additionally, the Pt/rGO/P3ABA-modified electrode revealed a lower R_{ct} (8.25 kΩ, curve e, Fig. 3(B)) than those of the Pt/P3ABA-modified SPCE and rGO/P3ABA-modified SPCE. Therefore, this result indicates that the combination of both PtNPs and rGO within nanocomposite can further reduce the electron transfer resistance, resulting in an enhanced electron transfer rate attributed to the better electrochemical activity and higher electroactive surface area.

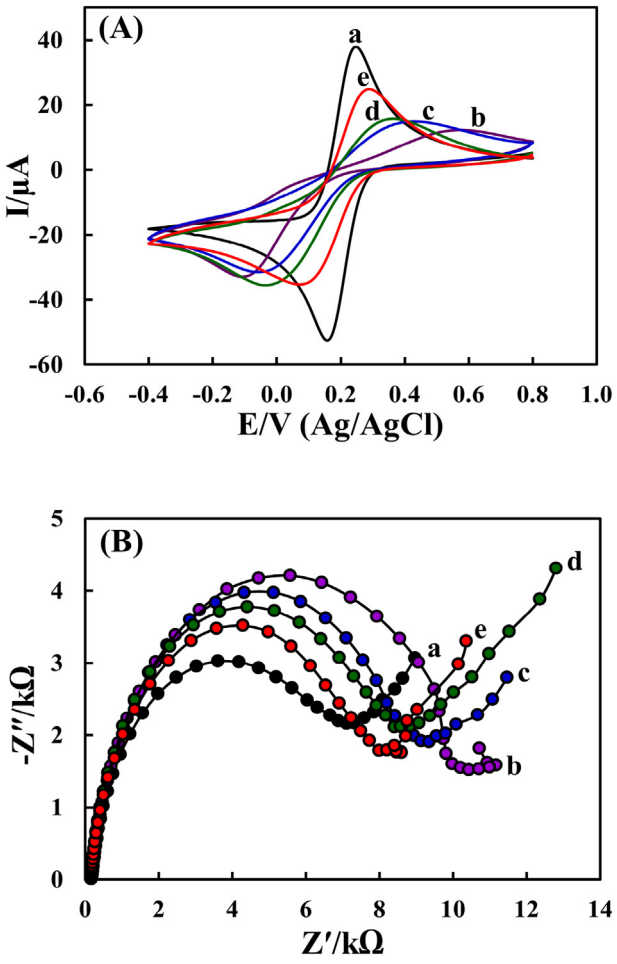

Fig. 3. CVs at a scan rate of 50 mV s^{-1} (A) and EIS spectra (B) of bare SPCE (a), P3ABA- (b), rGO/P3ABA- (c), Pt/P3ABA- (d), and Pt/rGO/P3ABA-modified (e) SPCEs in contact with 5.0 mM $K_3[Fe(CN)_6]$ solution containing 0.10 M KCl.

The electrochemical behavior of the Pt/rGO/P3ABA-modified electrode was examined using a standard solution of $K_3[Fe(CN)_6]$ as a redox couple probe. CV was performed at different scan rates in the range of 20–300 mV s^{-1}. The CV curves and the relationship between the current density and the square root of the scan rate are plotted in Fig. 4. It can be seen that the redox peak currents are gradually increased and that the peak positions are shifted slightly by increasing the scan rate. The plots of the peak current against the square root of the scan rate exhibited linear relationships with good correlation coefficients (R^2) of 0.992 and 0.995 for the anodic and cathodic peak currents, respectively, indicating that the redox behavior at the modified electrode is a diffusion-controlled process. The scan rate of 50 mV s^{-1} was selected to perform the measurement in this work. To confirm the presence of PtNPs within the nanocomposite, the electrochemical behavior

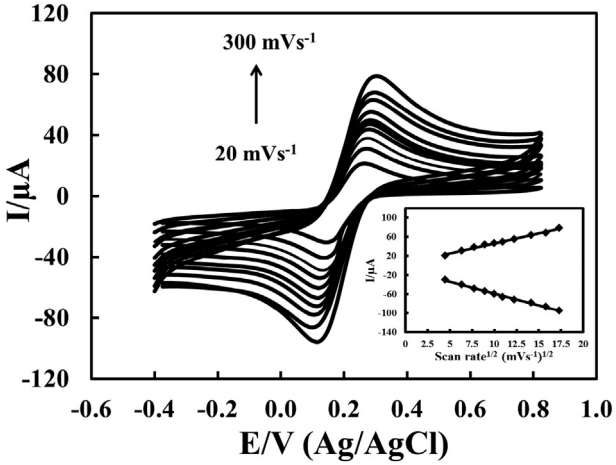

Fig. 4. CVs of the Pt/rGO/P3ABA nanocomposite-modified electrode in contact with 5.0 mM $K_3[Fe(CN)_6]$ solution containing 0.10 M KCl at different scan rates from 20 to 300 mV s^{-1} and the linear relationship between peak currents and the square root of scan rate (inset). The linear regression lines for anodic and cathodic peak currents have equations of y = 4.177 × + 4.4299 (R^2 = 0.992) and y = −4.9379 × − 9.7488 (R^2 = 0.995), respectively.

of the PtNPs in the modified electrode was investigated by CV in 0.50 M H_2SO_4, as shown in Fig. S6 (supporting information). The Pt/P3ABA-modified SPCE obviously exhibited the characteristic features of Pt related to its hydrogen adsorption/desorption (in the potential ranges from −0.26 to −0.18 V and − 0.16 to −0.24 V, respectively), elevated oxide formation region, and oxide reduction peak at the potential of 0.30 V (curve d, Fig. S6). Observable and significant hydrogen adsorption/desorption of Pt (in the potential ranges from −0.26 to 0.12 V and 0.08 to −0.22 V, respectively) and higher current densities of the Pt oxide formation and reduction were achieved for the Pt/rGO/P3ABA-modified SPCE (curve e, Fig. S6) compared to those of the SPCEs (curves a-c, Fig. S6), indicating that PtNPs were deposited together with rGO and P3ABA to form the film on the SPCE [36,54]. In addition, the reduction peak potential of Pt oxide for the Pt/rGO/P3ABA-modified SPCE shifted to 0.44 V.

3.3.2. Electrocatalytic performance of modified electrodes towards H_2O_2 oxidation

The catalytic performances of different modified electrodes towards the electrochemical oxidation of H_2O_2 were further investigated in PBS solution in the presence of 2.5 mM H_2O_2 using CV. The CV curves with different platforms are shown in Fig. S7(A). Although unmodified SPCE possesses a lower electron transfer resistance with the $K_3[Fe(CN)_6]$ redox probe, the result showed a very low catalytic current response to H_2O_2 (curve a, Fig. S7(A)). Additionally, the rGO/P3ABA- and P3ABA-modified SPCEs exhibited a similar trend with low responses (curves b and c, Fig. S7(A)), but the current responses from such electrodes are higher than that of a bare SPCE. This result suggests that the presence of rGO within the nanocomposite film can enhance the electroreactivity of the electrode surface. A small oxidation peak of H_2O_2 electrooxidation at the potential of +0.60 V (curve d, Fig. S7(A)) could be observed with respect to the Pt/P3ABA-modified SPCE, which is a unique electrocatalytic oxidation response of H_2O_2 over PtNPs. Interestingly, the Pt/rGO/P3ABA-modified SPCE clearly exhibited an excellent electrocatalysis of H_2O_2, with the remarkably high oxidation peak observed in the CV curve (curve e, Fig. S7(A)). Compared to the Pt/P3ABA- and rGO/P3ABA-modified SPCEs, the current response at the potential of +0.60 V for the Pt/rGO/P3ABA-modified SPCE was improved by approximately 5.75 and 13.14 times, respectively, indicating the synergistic effect of PtNPs and rGO. This combination offered both the best electrochemical oxidation and the highest sensitivity. In addition, an amperometric measurement of H_2O_2 oxidation at the modified electrodes was subsequently conducted for the successive addition of H_2O_2 solution into 0.10 M PBS (pH 7.4) under stirring and an applied potential of +0.50 V. Typical current-time responses are shown in Fig. S7 (B). It is found that the Pt/rGO/P3ABA sensing platform exhibited an excellent catalytic performance, indicating the highest sensitivity followed by that of the Pt/P3ABA-modified SPCE. Weak signals were obtained from the rGO/P3ABA-modified SPCE and P3ABA-modified SPCE, which were related to the previous CV results. According to the effective electrocatalytic property of the Pt/rGO/P3ABA-modified electrode, the detection of H_2O_2 was further evaluated with various concentrations (0–5.0 mM), as illustrated in Fig. 5. The increase in anodic current response was found by the increase in the H_2O_2 concentration.

Under optimized experimental conditions, the Pt/rGO/P3ABA sensing platform was consequently employed for the detection of H_2O_2 with successive additions, as shown in Fig. 6. The linear relationship between current response and concentration exhibited a good correlation coefficient (R^2) of 0.9927 over the concentration range of 0.010–0.80 mM, with a high sensitivity of 0.0835 μA μM^{-1} cm^{-2} and a low limit of detection (LOD) of 5.24 μM. The LOD of the proposed sensor was calculated using three standard deviations (SD_b) from the blank signal divided by the slope (m) of the calibration standard curve (LOD = $3SD_b/m$). The Pt/rGO/P3ABA nanocomposite-modified SPCE was further used in the development of glucose and cholesterol biosensors by the immobilization of GOx and ChOx onto the electrode surface, namely, GOx/Pt/rGO/P3ABA- and ChOx/Pt/rGO/P3ABA-modified SPCEs, respectively. The nanostructures possess an abundance of free carboxylic groups on the P3ABA polymer chain, which is favorable to form covalent bonds between the activated carboxylic groups and the amino groups of the enzymes. Additionally, rGO not only has gained a high conductivity in this system but also exhibits a large electroactive surface area, which would promote improved loading of immobilized enzymes, one of the most important factors affecting the performances of biosensors. Moreover, the distribution of PtNPs together with rGO in the developed platform also exhibits a unique electrocatalytic property towards H_2O_2, which is generated during both enzymatic reactions. Therefore, the synergistic effect in the nanocomposite could provide a great potential to efficiently detect H_2O_2, the production of which is proportional to the oxidation of the substrate (glucose or cholesterol) by enzymes (GOx or ChOx). Furthermore, the Pt/rGO/P3ABA film provides good charge transfer at the electrolyte/electrode interface.

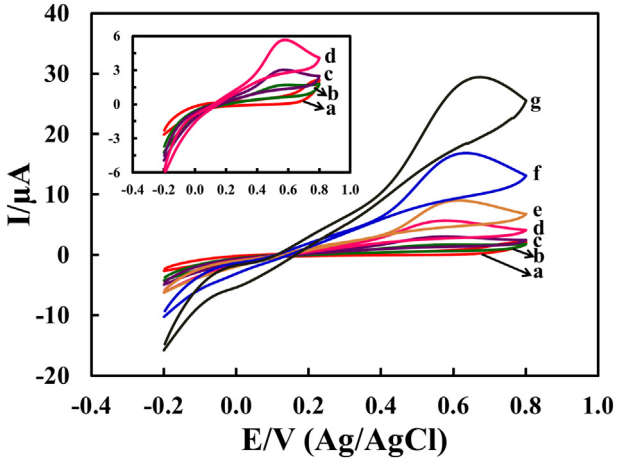

Fig. 5. CVs of the Pt/rGPO/P3ABA-modified SPCE in contact with 0.10 M PBS (pH 7.4) containing various concentrations of H_2O_2, (a) 0 mM, (b) 0.15 mM, (c) 0.30 mM, (d) 0.60 mM, (e) 1.25 mM, (f) 2.50 mM, and (g) 5.00 mM at a scan rate of 50 mV s^{-1}.

The electrocatalytic performances of glucose and cholesterol biosensors towards glucose and cholesterol have been demonstrated in Figs. S8(A) and S8(B), respectively (supporting information). The CVs for GOx/Pt/rGO/P3ABA- and ChOx/Pt/rGO/P3ABA-modified SPCEs in solutions containing glucose and cholesterol, respectively, revealed higher currents due to bioelectrocatalytic reactions. The currents are proportional to their concentrations, and the bioelectrocatalytic currents are increased by increasing the applied potential. At a low potential of

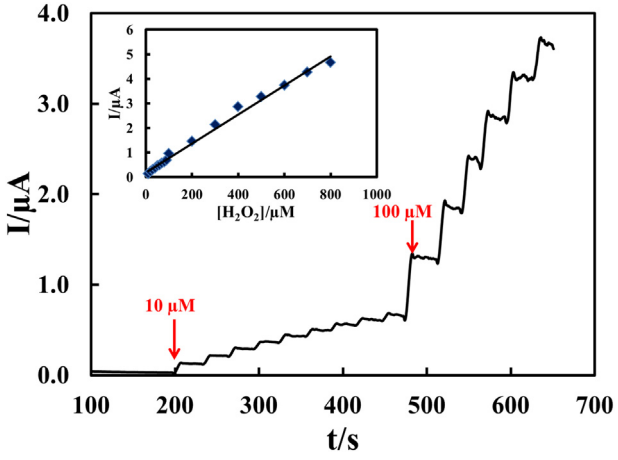

Fig. 6. Amperometric response of Pt/rGO/P3ABA/SPCE for detection of H_2O_2 in 0.10 M PBS (pH 7.4) and the calibration curve (inset). A linear regression line for the curve has an equation of y = 0.0059× + 0.1897 (R^2 = 0.9927).

+0.40 V, there is low sensitivity (low current response) in the case of both biosensors, and responses could not be discriminated between low and high concentrations of the analytes, while high sensitivities for the detection of both analytes were observed at high applied potentials such as +0.60, +0.70, and+0.80 V. Although high potential offers good sensitivity, the detection is affected by interfering currents from other electroactive species such as AA and UA. Therefore, +0.50 V was chosen as the working potential in order to reduce the interference effect from common electroactive species in our study.

3.3.3. Chronoamperometric determination of glucose and cholesterol

Chronoamperometry was widely applied to examine the quantification of glucose and cholesterol because of its high sensitivity [19]. The determination of glucose or cholesterol is based on the electrocatalysis current response of H_2O_2 produced from their enzymatic oxidations. In this work, the chronoamperometric measurement was performed at the constant potential of +0.50 V, with different standard concentrations, and the current responses could be recorded at the steady-state current of 50 s. For the glucose biosensor, chronoamperograms and the plot of current response against glucose concentration were obtained, as presented in Figs. 7(A) and 7(B). The result shows that the current response increases with increasing glucose concentration and slightly changes at high concentrations above 6.0 mM, at which access to the electrode surface could be limited. Our glucose biosensor exhibited a high sensitivity (22.01 μA.mM^{-1}.cm^{-2}), and the LOD was estimated to be 44.3 μM ($n = 3$). Additionally, the glucose biosensor provided an excellent linear response to glucose solutions in the range of concentrations from 0.25 to 6.00 mM ($R^2 = 0.9988$), with the relative standard deviations (RSDs) between 1.22% and 6.47% ($n = 3$). As seen in Table 1, the sensitivity of our sensor is greater than that of a PtNPs/nitrogen-doped GP nanoscroll-modified glassy carbon electrode (GCE) (6.36 μA mM^{-1} cm^{-2}) [29], while its linear dynamic range is wider than those of some previous reports: GP/conducting polyaniline-modified Pt electrode (0.010–1.48 mM) [17], Pt/GP/chitosan-modified GCE (0.15–5.0 mM) [45], and chitosan/rGO/AuNPs-modified Pt electrode (0.010–2.13 mM) [55].

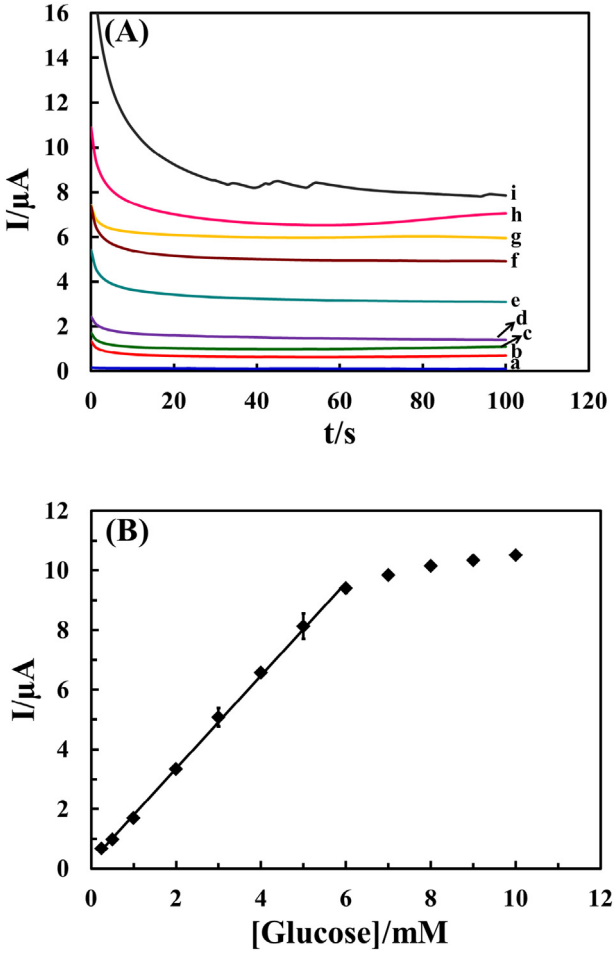

Fig. 7. (A) Chronoamperograms from different glucose concentrations, (a) 0 mM, (b) 0.25 mM, (c) 0.50 mM, (d) 1.00 mM, (e) 2.00 mM, (f) 3.00 mM, (g) 4.00 mM, (h) 5.00 mM, and (i) 6.00 mM using the Pt/rGO/P3ABA-modified electrode at an operating potential of +0.50 V in 0.10 M PBS (pH 7.4) and (B) the corresponding calibration curve of glucose determination. A linear regression line for the calibration curve has an equation of y = 1.5554× + 0.25 ($R^2 = 0.9988$).

Additionally, the fabricated cholesterol biosensor (ChOx/Pt/rGO/P3ABA-modified SPCE) demonstrated a similar trend to the glucose biosensor, with the current responses related to the concentration of cholesterol solution, as illustrated in Figs. 8(A) and 8(B). In Table 1, the excellent linear relationship of current response versus cholesterol concentration observed in our study is demonstrated in the range of 0.25–4.00 mM ($R^2 = 0.9928$) with the RSD between 0.12% and 6.61% ($n = 3$), which is wider than those based on a Pt/GP electrode (up to 35 μM) [18] and AuNPs/poly(diallyldimethylammonium chloride) (PDDA)/multiwalled carbon nanotube (MWCNT)-modified GCE (0.020–1.2 mM) [56]. Our cholesterol biosensor also obtained a low LOD of 40.5 μM ($n = 3$) and a good sensitivity of 15.94 μA mM^{-1} cm^{-2}, which are superior to those for the cholesterol biosensing based on a polyaniline/PtNPs electrode (0.88 μA mM^{-1} cm^{-2}) [1] and AuNPs/MWCNTs/polypyrrole-modified electrode (10.12 μA mM^{-1} cm^{-2}) [57].

The apparent Michaelis-Menten constant (K_m), which provides an indication of the enzyme-substrate kinetics, was calculated according to the Lineweaver-Burk equation [6,38,58]:

$$\frac{1}{I_{ss}} = \frac{1}{I_{max}} + \frac{K_m}{I_{max}} \times \frac{1}{C} \quad (1)$$

where I_{ss} is the steady-state current, I_{max} is the maximum current measured under the saturated substrate solution condition and C is the concentration of the substrate. Typically, the K_m value depends on the nature of the matrix or sensing platform and the immobilization process. The lower K_m value implies that a strong affinity between enzymes and substrates promoted effective enzymatic reaction [18]. The K_m of the fabricated glucose biosensor was estimated to be 3.54 mM, which was lower than that of free GOx in solution (27 mM) [59]. Furthermore, the K_m value demonstrates a much smaller magnitude than those of previous reports obtained from the glucose biosensors based on the Pt/mesoporous carbon CMK-3-modified GCE (10.8 mM) [60], AuNPs/PtNPs/CNT-modified Au electrode (10.73 mM) [61], rGO/PAMAM/AgNPs-modified GCE (9.64 mM) [62], polydopamine/GP-modified Au electrode (6.77 mM) [63], and chitosan/rGO/AuNPs-modified Pt electrode (4.33 mM) [55].

In the case of our fabricated cholesterol biosensor, the K_m value of ChOx was calculated to be 3.82 mM, which was higher than those observed by other cholesterol biosensing platforms such as PtPdNPs/chitosan/GP (0.11 mM) [16] and TiO_2/GP/PtPd/TiO_2-GP/AuNPs/ChOx (0.21 mM) [64]; however, the preparation of these materials involves high synthetic complexity and requires many chemicals. Furthermore, our biosensing platform provided a much lower K_m value than those reported in the literature, including the values obtained from cholesterol biosensors based on the PDDA/ChOx/MWCNTs-modified Au electrode [65], AgNPs/boron-doped diamond electrode coupled with PAD [66], and poly(3-thiopheneacetic acid)-modified Pt electrode [67], which were 7.17, 6.48, and 14.53 mM, respectively. The results above indicate that the immobilization of either GOx or ChOx onto the developed sensing platform demonstrated a good enzymatic activity and exhibited a high affinity to glucose and cholesterol, respectively. Furthermore, the comparison of the performances of our proposed glucose and cholesterol biosensors with those from the literature have been shown in Table 1, including the linear dynamic range, LOD, sensitivity, and K_m

Table 1
Comparison of the electrochemical biosensor performances of glucose and cholesterol biosensors with different modified electrodes based on nanomaterial and polymer.

Modified electrode[a]	linearity (mM)	Sensitivity (μA.mM^{-1}.cm^{2})	Detection limit (μM)	K_m (mM)	References
Glucose biosensor					
Pt/CMK-3-GOx-gelatin/GCE	0.04–12.2	ND	1	10.8	[60]
GOx/PtNP/PANI/PtE	0.01–8	96.1	0.7	2.35	[70]
GOD-CS/GP-PANI/Pt disc electrode	0.01–1.48	22.1	2.77	3.26	[17]
GOD/CS-rGO/AuNPs/Pt electrode	0.01–2.13	102.4	1.7	4.33	[55]
GOx/Pt/rGO/P3ABA/SPCE	0.25–6.00	22.01	44.3	3.54	This work
Cholesterol biosensor					
PDDA/ChOx/MWCNTs/AuE	up to 6.0 mM	7.32	200	7.17	[65]
ChOx/HRP/AuNPs/PDDA/MWCNTs/GCE	0.01–1.05	18.6	2.2	2.18	[56]
ChOx/AuNPs/PDDA/MWCNTs/GCE	0.02–1.2	2.23	4.4	0.89	[56]
ChOx/Poly(3TPAA)/PtE	0–8	4.49	420	14.53	[67]
ChOx/Pt/rGO/P3ABA/SPCE	0.25–4.00	15.94	40.5	3.82	This work

GCE: glassy carbon electrode, PtE: platinum electrode, AuE: gold electrode, NP: nanoparticle, Pt: platinum, CMK-3: mesoporous carbon CMK-3, PANI: polyaniline, rGO: reduced graphene oxide, CS: chitosan, PDDA: poly(diallyldimethylammonium chloride), MWCNT: multi-walled carbon nanotubes, AuNPs: gold nanoparticles, Poly(3TPAA): poly(3-thiopheneacetic acid).

value. The proposed platform for determination of glucose and cholesterol offers comparable device performances.

In summary for our Pt/rGO/P3ABA-modified SPCE, the presence of P3ABA provided a sufficient conductivity and a covalent attachment of enzymes, which protected against loss of enzyme to the electrolyte during measurement and preserved the enzyme activity similarly to that in a biological environment, while the PtNPs and rGO synergistically combined to yield high electroactive surface areas and electrocatalytic properties. Additionally, this sensing platform can be facilely fabricated in a one-step process, which reduced chemical usage and time consumption. This result suggests that the proposed sensing platform for biosensor device construction could be applied with low cost and high efficiency for the determination of glucose and cholesterol in clinical diagnostics.

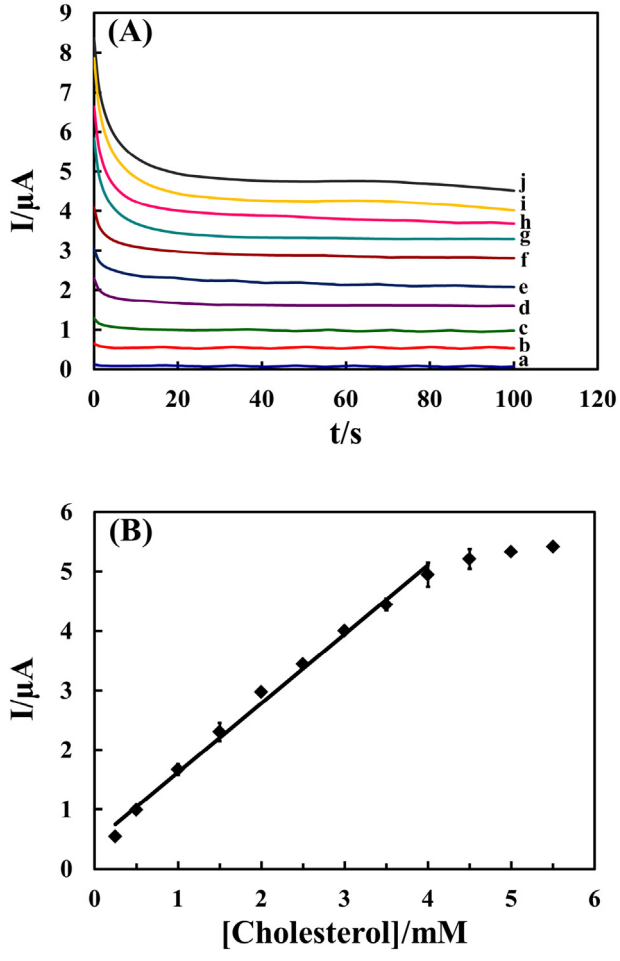

Fig. 8. (A) Chronoamperograms from different cholesterol concentrations, (a) 0 mM, (b) 0.25 mM, (c) 0.50 mM, (d) 1.00 mM, (e) 1.50 mM, (f) 2.00 mM, (g) 2.50 mM, (h) 3.00 mM, (i) 3.50 mM, and (j) 4.00 mM using the Pt/rGO/P3ABA-modified electrode at an operating potential of +0.50 V in 0.10 M PBS (pH 7.4) and (B) the calibration curve of cholesterol determination. A linear regression line for the calibration curve has an equation of $y = 1.1604\times + 0.4608$ ($R^2 = 0.9928$).

3.3.4. Interference study

Selectivity is a very important aspect of efficient biosensor detection of an analyte. In human body fluid, glucose (Glu) and cholesterol (Cho) are typically coexisting with common interfering molecules, some of which are electroactive compounds such as ascorbic acid (AA) and uric acid (UA) [2,55]. Therefore, the study of the interference effect on the determination of glucose and cholesterol was subsequently performed using chronoamperometry under the same experimental conditions. For the glucose biosensor, the interference effects of Cho (1.0 mM), AA (0.25 mM), UA (0.10 mM), and sucrose (Su) (1.0 mM) in the presence and absence of 1.0 mM glucose were investigated, and the effects on the current response of the proposed biosensor are shown in Fig. 9(A). In the case of the cholesterol biosensor, the current effects from Glu (1.0 mM), AA (0.25 mM), UA (0.10 mM), and sucrose (Su) (1.0 mM) with and without 1.0 mM cholesterol were also evaluated, as presented in Fig. 9(B). It was found that AA and UA strongly affected the current responses of both proposed biosensors (supporting information Fig. S9), but this problem was solved by coating the electrode with an anionic surfactant (SDS). In this study, 2.0 μL of 2.0 mM SDS was dropped onto the GOx/Pt/rGO/P3ABA- or ChOx/Pt/rGO/P3ABA-modified SPCE and then dried at room temperature before use. The anti-interference could be exhibited in the electrostatic repulsion between anionic SDS and anionic AA (p*Ka* = 4.1) and anionic UA (p*Ka* = 5.4) in neutral pH 7.4 [2,46]. As shown in Figs. 9(A) and 9(B), the interfering molecules can be oxidized at the applied operating potential of +0.50 V: especially UA and AA. The current responses from the electrochemical oxidation of AA and UA could contribute to the analytical responses for both glucose and cholesterol determinations. Compared to the responses of both enzymatic reactions using 1.0 mM glucose and 1.0 mM cholesterol, the currents from AA and UA oxidation are from 6.73–10.21%, which is significantly high; however, when the interferences coexisted in the detection solution with glucose or cholesterol, in the cases of Su, AA, UA, and Cho, the response differences were increased by approximately 0.59%, 2.94%, and 7.35% and decreased by approximately 4.41%, respectively, from the response of glucose alone. For the cholesterol detection system, the response differences were decreased by approximately 1.44% and 0.28%, and increased by approximately 4.35% and 8.40%, for the coexisting Glu, Su, AA, and UA, respectively. Although coexistence of the common interfering metabolites resulted in changes in the analytical response, a 10-fold higher concentration of substrate, i.e., glucose or

cholesterol, was employed in our study. In general, normal human plasma contains glucose (3.5–5.5 mM) [68], cholesterol (<5.17 mM) [1], UA (0.13–0.46 mM) [1], and AA (23 μM) [69]. The concentration of glucose is higher than those of UA (ca. 8–42 times) and AA (ca. 152–239 times), while the cholesterol concentration is higher than those of UA (ca. 11–40 times) and AA (ca. 225 times). Moreover, the concentrations of glucose and cholesterol are much higher in patients. This consideration suggests that no interference effect occurred when our biosensors were used for glucose and cholesterol assays. Therefore, the result indicates that by using our glucose and cholesterol biosensors, the interference effect is negligible. Consequently, our proposed biosensors provide a satisfactory selectivity and have an applicability to assay both analytes efficiently within real samples.

3.3.5. Reproducibility, repeatability, and stability of biosensors

The reproducibility, repeatability, and stability of proposed biosensors were also investigated using amperometric measurement under the optimized conditions. Sufficient reproducibility of each biosensor is obtained with current responses of five individual biosensors for each system, and 2.58% RSD ($n = 5$) and 3.50% RSD ($n = 5$) were observed for 1.0 mM glucose and cholesterol, respectively. Moreover, to investigate electrode reproducibility, five individual Pt/rGO/P3ABA/SPCEs were employed to detect 1.0 mM H_2O_2, and the RSD ($n = 5$) was calculated as 4.08%. The repeatability of each system is observed with 2.81% RSD ($n = 5$, 2.5 mM glucose) and 3.30% RSD ($n = 5$, 2.5 mM cholesterol) for the glucose and cholesterol biosensors, respectively, verifying the satisfactory repeatability of each biosensing system. To evaluate the stability of the prepared electrode and both biosensors, Pt/rGO/P3ABA-, GOx/Pt/rGO/P3ABA- and ChOx/Pt/rGO/P3ABA-modified SPCEs were stored at a temperature of 4.0 °C for 7 days, and changes in current responses towards 1.0 mM H_2O_2, 1.0 mM glucose, and 1.0 mM cholesterol, separately, were measured, as shown in Fig. S10. It was found that after 7 days, the storage electrodes retained the current responses of ca. 87, 86, and 88% of the initial responses for the detection of H_2O_2, glucose, and cholesterol, respectively. The results indicate the sufficient stability of these electrodes.

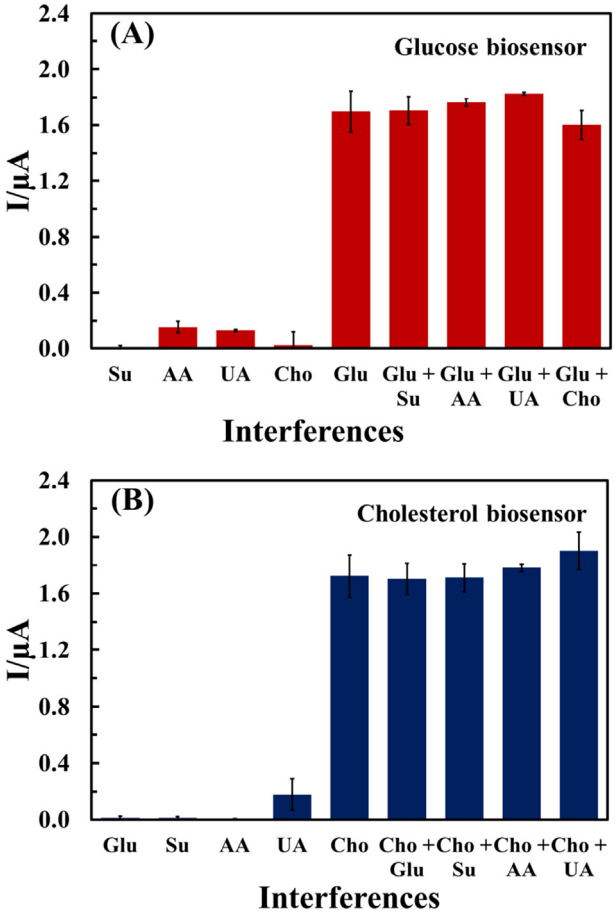

Fig. 9. Interference study of glucose (A) and cholesterol (B) biosensors.

Table 2
Determination of glucose and cholesterol in human serum samples ($n = 3$).

Glucose		
Added (mM)	Found (mM)	% Recovery
0.50	0.491 ± 0.030	98.2
1.00	1.028 ± 0.019	102.8
2.00	2.044 ± 0.134	102.2
Cholesterol		
0.50	0.493 ± 0.029	98.6
1.00	1.041 ± 0.092	104.1
2.00	2.010 ± 0.003	100.5

3.3.6. Sample analysis

Glucose and cholesterol levels, as indicative biomarkers, are important factors to estimate human health and diagnosis disease. To study the possibilities of clinical application, the proposed biosensors were applied in the determination of glucose and cholesterol in a human serum sample. Different concentrations of glucose or cholesterol (0.50, 1.00, and 2.00 mM) were spiked into a 50-fold diluted human serum, and the result of this recovery study is shown in Table 2. The percentages of recoveries were observed in the ranges of 98.2–102.8% and 98.6–104.1% for glucose and cholesterol biosensors, respectively. This result suggests that the proposed biosensor could be employed to measure glucose and cholesterol within clinical samples.

4. Conclusions

In summary, a Pt/rGO/P3ABA nanocomposite film on SPCE was successfully synthesized using a facile one-step electrochemical deposition. The Pt/rGO/P3ABA-modified SPCE exhibited an excellent electrocatalytic capability towards H_2O_2 oxidation. Therefore, our novel and versatile sensing platform was examined in terms of applicability in the fabrication of glucose and cholesterol biosensors by immobilizing GOx and ChOx onto the surface of the modified electrode, respectively. These biosensors achieved excellent sensing capabilities in the detection of both metabolites, with wide linear dynamic ranges, high sensitivity, and low detection limits. Furthermore, the biosensors possessed good anti-interference ability, thus exhibiting suitability for genuine sample analysis in clinical diagnosis. Moreover, our versatile Pt/rGO/P3ABA-modified SPCE offers a great potential use for the construction of other biosensors by using other specific enzymes, for example, uricase, lactate oxidase, and alcohol oxidase.

Acknowledgments

This work was supported by the Science Achievement Scholarship of Thailand (SAST) and by the National Nanotechnology Center (NANOTEC), the National Science and Technology Development Agency (NSTDA), Thailand. This research work was partially supported by Chiang Mai University. The authors gratefully acknowledge the Graduate School (Chiang Mai University), the Research Center on Chemistry for Development of Health Promoting Products from Northern Resources, the Center of Excellence for Innovation in Chemistry (PERCH-CIC), and the Department of Chemistry, Faculty of Science, Chiang Mai University.

Appendix A. Supplementary data

Supplementary data to this article can be found online at https://doi.org/10.1016/j.bioelechem.2019.01.008.

References

[1] L. Li, Y. Wang, L. Pan, Y. Shi, W. Cheng, Y. Shi, G. Yu, A nanostructured conductive hydrogels-based biosensor platform for human metabolite detection, Nano Lett. 15 (2015) 1146–1151.

[2] R.S. Dey, C.R. Raj, Redox-functionalized graphene oxide architecture for the development of amperometric biosensing platform, ACS Appl. Mater. Interfaces 5 (2013) 4791–4798.

[3] J. Huang, Y. Liu, P. Zhang, Y. Li, L. Ding, A temperature-triggered fiber optic biosensor based on hydrogel-magnetic immobilized enzyme complex for sequential determination of cholesterol and glucose, Biochem. Eng. J. 125 (2017) 123–128.

[4] K. Dhara, J.R.T. Stanley, B.G.S.T. Nari, Pt-CuO nanoparticles decorated reduced graphene oxide for the fabrication of highly sensitive non-enzymatic disposable glucose sensor, Sensors Actuators B Chem. 195 (2014) 197–205.

[5] C. Hu, D.-P. Yang, F. Zhu, F. Jiang, S. Shen, J. Zhang, Enzyme-labeled Pt@BSA nanocomposite as a facile electrochemical biosensing interface for sensitive glucose determination, ACS Appl. Mater. Interfaces 6 (2014) 4170–4178.

[6] S. Nantaphol, O. Chailapakul, W. Siangproh, Sensitive and selective electrochemical sensor using silver nanoparticles modified glassy carbon electrode for determination of cholesterol in bovine serum, Sensors Actuators B Chem. 207 (2015) 193–198.

[7] P.J. Lamas-Ardisana, G. Martínez-Paredes, L. Añorga, H.J. Grande, Glucose biosensor based on disposable electrochemical paper-based transducers fully fabricated by screen-printing, Biosens. Bioelectron. 109 (2018) 8–12.

[8] A. Gorassini, G. Verardo, S.-C. Fregolent, R. Bortolomeazzi, Rapid determination of cholesterol oxidation products in milk powder based products by reversed phase SPE and HPLC-APCI-MS/MS, Food Chem. 230 (2017) 604–610.

[9] M. Filip, M. Vlassa, V. Coman, A. Halmagyi, Simultaneous determination of glucose, fructose, sucrose and sorbitol in the leaf and fruit peel of different apple cultivars by the HPLC–RI optimized method, Food Chem. 199 (2016) 653–659.

[10] C. Ma, Z. Sun, C. Chen, L. Zhang, S. Zhu, Simultaneous separation and determination of fructose, sorbitol, glucose and sucrose in fruits by HPLC–ELSD, Food Chem. 145 (2014) 784–788.

[11] L. Su, J. Feng, X. Zhou, C. Ren, H. Li, X. Chen, Colorimetric detection of urine glucose based on $ZnFe_2O_4$ magnetic nanoparticles, Anal. Chem. 84 (2012) 5753–5758.

[12] J. Chitra, M. Ghosh, H.N. Mishra, Rapid quantification of cholesterol in dairy powders using Fourier transform near infrared spectroscopy and chemometrics, Food Control 78 (2017) 342–349.

[13] X. Wu, Y. Chai, R. Yuan, X. Zhong, J. Zhang, Synthesis of multiwall carbon nanotubes-graphene oxide-thionine-Au nanocomposites for electrochemiluminescence detection of cholesterol, Electrochim. Acta 129 (2014) 441–449.

[14] X.-m. Chen, Z.-m. Cai, Z.-j. Lin, T.-t. Jia, H.-z. Liu, Y.-q. Jiang, X. Chen, A novel non-enzymatic ECL sensor for glucose using palladium nanoparticles supported on functional carbon nanotubes, Biosens. Bioelectron. 24 (2009) 3475–3480.

[15] G. Maduraiveeran, M. Sasidharan, V. Ganesan, Electrochemical sensor and biosensor platforms based on advanced nanomaterials for biological and biomedical applications, Biosens. Bioelectron. 103 (2018) 113–129.

[16] S. Cao, L. Zhang, Y. Chai, R. Yuan, Electrochemistry of cholesterol biosensor based on a novel Pt–Pd bimetallic nanoparticle decorated graphene catalyst, Talanta 109 (2013) 167–172.

[17] X. Feng, H. Cheng, Y. Pan, H. Zheng, Development of glucose biosensors based on nanostructured graphene-conducting polyaniline composite, Biosens. Bioelectron. 70 (2015) 411–417.

[18] R.S. Dey, C.R. Raj, Development of an amperometric cholesterol biosensor based on graphene−Pt nanoparticle hybrid material, J. Phys. Chem. C 114 (2010) 21427–21433.

[19] A. Safavi, F. Farjami, Electrodeposition of gold–platinum alloy nanoparticles on ionic liquid–chitosan composite film and its application in fabricating an amperometric cholesterol biosensor, Biosens. Bioelectron. 26 (2011) 2547–2552.

[20] X.-M. Feng, R.-M. Li, Y.-W. Ma, R.-F. Chen, N.-E. Shi, Q.-L. Fan, W. Huang, One-step electrochemical synthesis of graphene/polyaniline composite film and its applications, Adv. Funct. Mater. 21 (2011) 2989–2996.

[21] M. Lv, Y. Liu, J. Geng, X. Kou, Z. Xin, D. Yang, Engineering nanomaterials-based biosensors for food safety detection, Biosens. Bioelectron. 106 (2018) 122–128.

[22] P. Chaturvedi, D.C. Vanegas, M. Taguchi, S.L. Burrs, P. Sharma, E.S. McLamore, A nanoceria–platinum–graphene nanocomposite for electrochemical biosensing, Biosens. Bioelectron. 58 (2014) 179–185.

[23] J.-D. Qiu, G.-C. Wang, R.-P. Liang, X.-H. Xia, H.-W. Yu, Controllable deposition of platinum nanoparticles on graphene as an electrocatalyst for direct methanol fuel cells, J. Phys. Chem. C 115 (2011) 15639–15645.

[24] S. Stankovich, D.A. Dikin, R.D. Piner, K.A. Kohlhaas, A. Kleinhammes, Y. Jia, Y. Wu, S.B.T. Nguyen, R.S. Ruoff, Synthesis of graphene-based nanosheets via chemical reduction of exfoliated graphite oxide, Carbon 45 (2007) 1558–1565.

[25] C. Liu, C. He, T. Xie, J. Yang, Reduction of graphite oxide using ammonia solution and detection Cr(VI) with graphene-modified electrode fullerenes, Nanotubes, Carbon Nanostruct. 23 (2015) 125–130.

[26] V. Dua, S.P. Surwade, S. Ammu, S.R. Agnihotra, S. Jain, K.E. Roberts, S. Park, R.S. Ruoff, S.K. Manohar, All-organic vapor sensor using inkjet-printed reduced graphene oxide, Angew. Chem. Int. Ed. 49 (2010) 2154–2157.

[27] G. Wang, J. Yang, J. Park, X. Gou, B. Wang, H. Liu, J. Yao, Facile synthesis and characterization of graphene nanosheets, J. Phys. Chem. C 112 (2008) 8192–8195.

[28] O. Akhavan, E. Ghaderi, S. Aghayee, Y. Fereydooni, A. Talebi, The use of a glucose-reduced graphene oxide suspension for photothermal cancer therapy, J. Mater. Chem. 22 (2012) 13773–13781.

[29] L. Meng, Y. Xia, W. Liu, L. Zhang, P. Zou, Y. Zhang, Hydrogen microexplosion synthesis of platinum nanoparticles/nitrogen doped graphene nanoscrolls as new amperometric glucose biosensor, Electrochim. Acta 152 (2015) 330–337.

[30] R.M. Alonso, M.I. San-Martín, A. Sotres, A. Escapa, Graphene oxide electrodeposited electrode enhances start-up and selective enrichment of exoelectrogens in bioelectrochemical systems, Sci. Rep. 7 (2017), 13726.

[31] Y. Shang, D. Zhang, Y. Liu, C. Guo, Preliminary comparison of different reduction methods of graphene oxide, Bull. Mater. Sci. 38 (2015) 7–12.

[32] J.A. Bennett, I.B. Agbere, M. Moesta, Complete coating of underlying Pt electrodes by electrochemical reduction of graphene oxide, Electrochim. Acta 188 (2016) 111–119.

[33] G.-T. Liu, H.-F. Chen, G.-M. Lin, P.-p. Ye, X.-P. Wang, Y.-Z. Jiao, X.-Y. Guo, Y. Wen, H.-F. Yang, One-step electrodeposition of graphene loaded nickel oxides nanoparticles for acetaminophen detection, Biosens. Bioelectron. 56 (2014) 26–32.

[34] F. Xu, Y. Sun, Y. Zhang, Y. Shi, Z. Wen, Z. Li, Graphene–Pt nanocomposite for nonenzymatic detection of hydrogen peroxide with enhanced sensitivity, Electrochem. Commun. 13 (2011) 1131–1134.

[35] Y. Zhang, X. Bai, X. Wang, K.-K. Shiu, Y. Zhu, H. Jiang, Highly sensitive graphene–Pt nanocomposites amperometric biosensor and its application in living cell H_2O_2 detection, Anal. Chem. 86 (2014) 9459–9465.

[36] S. Guo, D. Wen, Y. Zhai, S. Dong, E. Wang, Platinum nanoparticle ensemble-on-graphene hybrid nanosheet: one-pot, rapid synthesis, and used as new electrode material for electrochemical sensing, ACS Nano 4 (2010) 3959–3968.

[37] Y. Sun, K. He, Z. Zhang, A. Zhou, H. Duan, Real-time electrochemical detection of hydrogen peroxide secretion in live cells by Pt nanoparticles decorated graphene–carbon nanotube hybrid paper electrode, Biosens. Bioelectron. 68 (2015) 358–364.

[38] S. Pakapongpan, R.P. Poo-arporn, Self-assembly of glucose oxidase on reduced graphene oxide-magnetic nanoparticles nanocomposite-based direct electrochemistry for reagentless glucose biosensor, Mater. Sci. Eng. C 76 (2017) 398–405.

[39] Q. Xu, S.-X. Gu, L. Jin, Y. Zhou, Z. Yang, W. Wang, X. Hu, Graphene/polyaniline/gold nanoparticles nanocomposite for the direct electron transfer of glucose oxidase and glucose biosensing, Sensors Actuators B Chem. 190 (2014) 562–569.

[40] F.E. Kanik, E. Rende, S. Timur, L. Toppare, A novel functional conducting polymer: synthesis and application to biomolecule immobilization, J. Mater. Chem. 22 (2012) 22517–22525.

[41] A. Berkkan, A.İ. Seçkin, K. Pekmez, U. Tamer, Amperometric enzyme electrode for glucose determination based on poly(pyrrole-2-aminobenzoic acid), J, Solid State Electrochem 14 (2010) 975–980.

[42] K.-J. Huang, Q.-S. Jing, Z.-W. Wu, L. Wang, C.-Y. Wei, Enhanced sensing of dopamine in the present of ascorbic acid based on graphene/poly(p-aminobenzoic acid) composite film, Colloids Surf. B: Biointerfaces 88 (2011) 310–314.

[43] A. Liu, S. Huang, A glucose biosensor based on direct electrochemistry of glucose oxidase immobilized onto platinum nanoparticles modified graphene electrode, Sci. China Phys. Mech. 55 (2012) 1163–1167.

[44] Z. Li, C. Xie, J. Wang, A. Meng, F. Zhang, Direct electrochemistry of cholesterol oxidase immobilized on chitosan–graphene and cholesterol sensing, Sensors Actuators B Chem. 208 (2015) 505–511.

[45] H. Wu, J. Wang, X. Kang, C. Wang, D. Wang, J. Liu, I.A. Aksay, Y. Lin, Glucose biosensor based on immobilization of glucose oxidase in platinum nanoparticles/graphene/chitosan nanocomposite film, Talanta 80 (2009) 403–406.

[46] N. Ruecha, R. Rangkupan, N. Rodthongkum, O. Chailapakul, Novel paper-based cholesterol biosensor using graphene/polyvinylpyrrolidone/polyaniline nanocomposite, Biosens. Bioelectron. 52 (2014) 13–19.

[47] W.S. Hummers Jr., R.E. Offeman, Preparation of graphitic oxide, J. Am. Chem. Soc. 80 (1958) 1339.

[48] Y.-C. Tsai, S.-Y. Chen, C.-A. Lee, Amperometric cholesterol biosensors based on carbon nanotube–chitosan–platinum–cholesterol oxidase nanobiocomposite, Sensors Actuators B Chem. 135 (2008) 96–101.

[49] P. Netsuwan, W. Chaisu, S. Phanichphant, S. Sriwichai, Nanocomposite thin film of poly(3-aminobenzoic acid) and multiwalled carbon nanotubes fabricated through an electrochemical method, Adv. Mater. Sci. Eng. 2014 (2014) 1–6.

[50] S. Sriwichai, R. Janmanee, S. Phanichphant, K. Shinbo, K. Kato, F. Kaneko, T. Yamamoto, A. Baba, Development of an electrochemical-surface plasmon dual biosensor based on carboxylated conducting polymer thin films, J. Appl. Polym. Sci. 135 (2018), 45641.

[51] N. Huang, M. Liu, H. Li, Y. Zhang, S. Yao, Synergetic signal amplification based on electrochemical reduced graphene oxide-ferrocene derivative hybrid and gold nanoparticles as an ultra-sensitive detection platform for bisphenol A, Anal. Chim. Acta 853 (2015) 249–257.

[52] A. Aghaei, M.R.M. Hosseini, M. Najafi, A novel capacitive biosensor for cholesterol assay that uses an electropolymerized molecularly imprinted polymer, Electrochim. Acta 55 (2010) 1503–1508.

[53] H. Liu, C. Tao, Z. Hu, S. Zhang, J. Wang, Y. Zhan, An electrochemical glucose biosensor based on graphene composites: use of dopamine as reducing monomer and as site for covalent immobilization of enzyme, RSC Adv. 4 (2014) 43624–43629.

[54] M.M. Pereira Silva Neves, M.B. González-García, P. Bobes-Limenes, A. Pérez-Junquera, D. Hernández-Santos, F.J. Vidal-Iglesias, J. Solla-Gullón, P. Fanjul-Bolado, A non-enzymatic ethanol sensor based on a nanostructured catalytic disposable electrode, Anal. Methods 9 (2017) 5108–5114.

[55] Y. Fang, D. Zhang, Y. Guo, Y. Guo, Q. Chen, Simple one-pot preparation of chitosan-reduced graphene oxide-Au nanoparticles hybrids for glucose sensing, Sensors Actuators B Chem. 221 (2015) 265–272.

[56] M. Eguílaz, R. Villalonga, L. Agüí, P. Yáñez-Sedeño, J.M. Pingarrón, Gold nanoparticles: poly(diallyldimethylammonium chloride)–carbon nanotubes composites as platforms for the preparation of electrochemical enzyme biosensors: application to the determination of cholesterol, J. Electroanal. Chem. 661 (2011) 171–178.

[57] M. Alagappan, S. Immanuel, R. Sivasubramanian, A. Kandaswamy, Development of cholesterol biosensor using Au nanoparticles decorated *f*-MWCNT covered with polypyrrole network, Arab. J. Chem. (2018) (In press).

[58] M. Dixon, The determination of enzyme inhibitor constants, Biochem. J. 55 (1953) 170–171.
[59] M.J. Rogers, K.G. Brandt, Interaction of D-glucal with Aspergillus Niger glucose oxidase, Biochemistry 10 (1971) 4624–4630.
[60] J. Yu, D. Yu, T. Zhao, B. Zeng, Development of amperometric glucose biosensor through immobilizing enzyme in a Pt nanoparticles/mesoporous carbon matrix, Talanta 74 (2008) 1586–1591.
[61] X. Chu, D. Duan, G. Shen, R. Yu, Amperometric glucose biosensor based on electrodeposition of platinum nanoparticles onto covalently immobilized carbon nanotube electrode, Talanta 71 (2007) 2040–2047.
[62] Z. Luo, L. Yuwen, Y. Han, J. Tian, X. Zhu, L. Weng, L. Wang, Reduced graphene oxide/PAMAM–silver nanoparticles nanocomposite modified electrode for direct electrochemistry of glucose oxidase and glucose sensing, Biosens. Bioelectron. 36 (2012) 179–185.
[63] C. Ruan, W. Shi, H. Jiang, Y. Sun, X. Liu, X. Zhang, Z. Sun, L. Dai, D. Ge, One-pot preparation of glucose biosensor based on polydopamine–graphene composite film modified enzyme electrode, Sensors Actuators B Chem. 177 (2013) 826–832.
[64] S. Cao, L. Zhang, Y. Chai, R. Yuan, An integrated sensing system for detection of cholesterol based on TiO2–graphene–Pt–Pd hybridnanocomposites, Biosens. Bioelectron. 42 (2013) 532–538.
[65] M. Guo, J. Chen, J. Li, L. Nie, S. Yao, Carbon nanotubes-based amperometric cholesterol biosensor fabricated through layer-by-layer technique, Electroanalysis 16 (2004) 1992–1998.
[66] S. Nantaphol, O. Chailapakul, W. Siangproh, A novel paper-based device coupled with a silver nanoparticle-modified boron-doped diamond electrode for cholesterol detection, Anal. Chim. Acta 891 (2015) 136–143.
[67] P.-C. Nien, P.-Y. Chen, K.-C. Ho, Fabricating an amperometric cholesterol biosensor by a covalent linkage between poly(3-thiopheneacetic acid) and cholesterol oxidase, Sensors 9 (2009) 1794–1806.
[68] M. Güemes, S.A. Rahman, K. Hussain, What is a normal blood glucose? Arch. Dis. Child. 0 (2015) 1–6.
[69] H.R. Jamaati, P. Pajouh, M. Nayebi, N. Baghaie, N. Baghaie, H. Khosravani, Ascorbic acid concentration in plasma and white blood cells of patients with bronchial asthma, Tanaffos 5 (2006) 29–35.
[70] D. Zhai, B. Liu, Y. Shi, L. Pan, Y. Wang, W. Li, R. Zhang, G. Yu, Highly sensitive glucose sensor based on Pt nanoparticle/polyaniline hydrogel heterostructures, ACS Nano 7 (2013) 3540–3546.